

HIGH-DIMENSIONAL BAYESIAN OPTIMISATION WITH GAUSSIAN PROCESS PRIOR VARIATIONAL AUTOENCODERS

Anonymous authors

Paper under double-blind review

ABSTRACT

Bayesian optimisation (BO) using a Gaussian process (GP)-based surrogate model is a powerful tool for solving black-box optimisation problems but does not scale well to high-dimensional data. Previous works have proposed to use variational autoencoders (VAEs) to project high-dimensional data onto a low-dimensional latent space and to implement BO in the inferred latent space. In this work, we propose a conditional generative model for efficient high-dimensional BO that uses a GP surrogate model together with GP prior VAEs. A GP prior VAE extends the standard VAE by conditioning the generative and inference model on auxiliary covariates, capturing complex correlations across samples with a GP. Our model incorporates the observed target quantity values as auxiliary covariates learning a structured latent space that is better suited for the GP-based BO surrogate model. It handles partially observed auxiliary covariates using a unifying probabilistic framework and can also incorporate additional auxiliary covariates that may be available in real-world applications. We demonstrate that our method improves upon existing latent space BO methods on simulated datasets as well as on commonly used benchmarks.

1 INTRODUCTION

Bayesian optimisation (BO) (Mockus, 1989; Shahriari et al., 2015; Frazier, 2018) is a technique for complex optimisation problems, where the true functional form of a target quantity of interest is unknown. This target quantity may be expensive to compute or may require time consuming experiments to obtain its value. Hence, one would like to minimise the number of evaluations that are required to optimise it. Although BO offers an approach for black-box optimisation problems, it does not efficiently scale to high-dimensional data settings (Shahriari et al., 2015).

Variational autoencoders (VAEs) (Kingma & Welling, 2014; Rezende et al., 2014) are a popular family of latent-variable models that are often used to learn low-dimensional representations of high-dimensional data. The low-dimensional latent space afforded by VAEs, that is representative of the high-dimensional, potentially discrete-valued data on which it is trained, offers a powerful scaling strategy for BO. BO is performed on the inferred low-dimensional continuous-valued manifold instead of the high-dimensional data space (Gómez-Bombarelli et al., 2018). This method of combining the benefits of VAEs with BO, known as VAE BO, is a general-purpose high-dimensional black-box optimisation method with many practical applications, such as molecule discovery (Gómez-Bombarelli et al., 2018; Griffiths & Hernández-Lobato, 2020; Jin et al., 2018), neural architecture search (Kandasamy et al., 2018; Ru et al., 2021) and chemical synthesis (Felton et al., 2020; Shields et al., 2021; Korovina et al., 2020).

Sohn et al. (2015) proposed conditional VAEs (cVAEs) as an extension that conditions a generative model on auxiliary covariates. However, similar to standard VAEs, this family of models ignores possible correlations between data samples. The Gaussian process (GP) prior VAE (Casale et al., 2018) extends the conditional VAE framework by replacing the i.i.d. standard Gaussian prior on the latent variables with a GP prior in order to capture arbitrary, but preferably smooth, correlations between data samples. These models have been shown to compare favourably to VAEs and cVAEs as well as effectively handle missing data in the observations. Ramchandran et al. (2024) introduced a

054
055
056
057
058
059
060
061
062
063
064
065
066
067
068
069
070
071
072
073
074
075
076
077
078
079
080
081
082
083
084
085
086
087
088
089
090
091
092
093
094
095
096
097
098
099
100
101
102
103
104
105
106
107

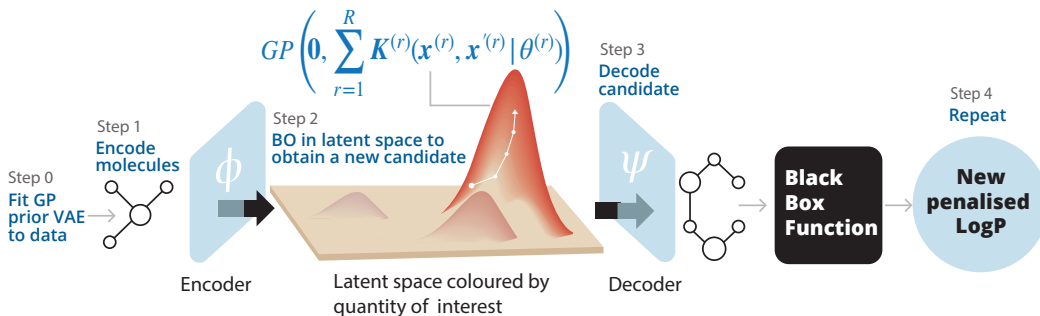


Figure 1: *An overview of our model.* Consider the example application of discovering novel drug-like molecules. Our method uses a GP prior VAE with an additive kernel over various partially observed auxiliary covariates such as molecular weight, number of hydrogen bonds, total polar surface area, etc. and the partially observed quantity of interest (represented by $x^{(r)}$ in this image for the r^{th} additive kernel) to learn a structured latent space. The black-box function evaluates the quantity of interest for the chosen molecule.

method to impute the missing auxiliary covariates in cVAEs and thereby enhance their applicability to real-world datasets.

Our Contribution We propose a novel conditional deep generative model for high-dimensional BO that improves upon the existing VAE BO methods. Our proposed model uses a GP prior VAE to learn a low-dimensional, structured latent representation of the data samples, and implements the GP surrogate model to optimise the target quantity (or quantities) of interest in the repeatedly re-trained latent space. We use these partially observed target quantity values directly as auxiliary covariates to condition the GP prior VAE model. The model also incorporates additional (partially or fully) observed auxiliary covariates that may be available for a given application. Furthermore, it can effectively handle missing values in both the high-dimensional observations as well as the auxiliary covariates using a principled technique that is particularly developed for learning conditional VAEs. Fig. 1 summarises our model.

Our contributions can be summarised as follows:

- We introduce a conditional VAE-based method for efficiently performing Bayesian optimisation on high-dimensional datasets.
- We learn structured latent representations of high-dimensional data points using a GP prior VAE that handle missing values in the observations, target quantity values, and in other possible auxiliary covariates.
- We demonstrate the efficacy of our method on a synthetic dataset and on common benchmarks.

2 RELATED WORKS

Bayesian optimisation is a popular black-box optimisation technique that is challenging to scale to high-dimensional data (Mockus, 1989; Shahriari et al., 2015; Frazier, 2018). (Binois & Wycoff, 2022) reviews the recent advancements in improving the efficiency of Bayesian Optimisation (BO) for high-dimensional problems, particularly through various structural model assumptions. To address the curse of dimensionality, Griffiths & Hernández-Lobato (2020) uses an autoencoder to learn a low-dimensional, non-linear manifold to scale BO to high-dimensional datasets. They perform a constrained BO over the latent space in order to incorporate the application-specific idiosyncrasies and thereby generate a high proportion of valid reconstructions. Stanton et al. (2022) integrate Denoising Autoencoders with a discriminative multi-task Gaussian process head into BO to learn a latent space that captures meaningful features of biological sequences. As autoencoders cannot be

The source code is available at *anonymised link*.

used to sample novel observations from their representation space, VAEs are an approach to make it possible to leverage the low-dimensional latent representation for generative purposes (Kusner et al., 2017; Gómez-Bombarelli et al., 2018). However, a vanilla VAE BO is sub-optimal as the learnt latent space is not constructed by leveraging the black-box function labels (Urtasun & Darrell, 2007; Siivola et al., 2021; Grosnit et al., 2021). Building upon this, some methods: use an automatic statistician perspective by learning the kernel combination of the surrogate GP (Lu et al., 2018), use manifold GPs in the encoder and manifold multi-output GPs in the decoder (Moriconi et al., 2020), reformulate the encoder to effectively act both as the encoder for the VAE as well as a deep kernel for the surrogate model within a local Bayesian optimisation framework using trust region method (Maus et al., 2022), and use label guidance in the latent space (Eissman et al., 2018; Tripp et al., 2020; Maus et al., 2022). Furthermore, Grosnit et al. (2021) proposed a method that combines VAEs with deep metric learning. They make use of label guidance from the labelled data points by incorporating various metric losses (e.g., triplet loss, contrasting loss, log ratio loss, etc.). However, this method does not incorporate additional information in the form of auxiliary covariates and the triplet loss requires an additional matching procedure as a pre-processing step, which can be time consuming.

Variational autoencoders (Kingma & Welling, 2014; Rezende et al., 2014) are popular deep learning methods that map high-dimensional, complex data to a low-dimensional space and vice-versa. Most VAE-based models assume the data to be fully observed or choose to substitute unobserved values of the encoder input with zeros (Nazabal et al., 2020; Mattei & Frellesen, 2019). Conditional variational autoencoders (Sohn et al., 2015) include information about the auxiliary covariates into both the inference and generative networks. Building upon this idea, Gaussian process prior VAEs have been proposed as an extension to incorporate arbitrary correlations as well as auxiliary covariates via Gaussian process priors (Casale et al., 2018; Fortuin et al., 2020; Ramchandran et al., 2021). These methods have shown competitive performance as well as handle missing values in the observed data. Ramchandran et al. (2024) proposed a conditional VAE-based learning approach that can robustly handle missing values in the auxiliary covariates.

3 BACKGROUND

Throughout the paper, we use the following notation: $\mathbf{y} \in \mathcal{Y}$ is a high-dimensional observation, $c \in \mathbb{R}$ is the target quantity that we want to optimise, $\mathbf{x} = [x_1, \dots, x_Q] \in \mathcal{X}$ denotes additional auxiliary covariates, and $\mathbf{z} \in \mathcal{Z} = \mathbb{R}^L$ is a L -dimensional latent variable. We define $\tilde{\mathbf{x}} = [c, \mathbf{x}] \in \mathbb{R} \times \mathcal{X}$. A set of N observations is denoted as $Y = [\mathbf{y}_1, \dots, \mathbf{y}_N]$, with X , \tilde{X} , and Z defined analogously. The target quantity $\mathbf{c} = [c_1, \dots, c_N]^T$ is typically partially observed.

3.1 BAYESIAN OPTIMISATION

Bayesian optimisation is a technique for performing efficient global optimisation of black-box functions (or unknown scoring functions) that are difficult to compute and whose functional form may not be known (Mockus, 1989; Frazier, 2018). Given a function $f : \mathcal{Y} \mapsto \mathbb{R}$ we aim to find a point $\mathbf{y} \in \mathcal{Y}$ that corresponds to the global optimum of f . The black-box function f is also referred to as a utility function as it is a measure of the target quantity, $c = f(\mathbf{y})$, that we are trying to optimise and informs us on the quality of the chosen sample. The problem can be written as (assuming maximisation), $\mathbf{y}^* = \arg \max_{\mathbf{y} \in \mathcal{Y}} f(\mathbf{y})$. Since, the unknown function f is assumed to be difficult or expensive to evaluate, Bayesian optimisation requires a surrogate model to model the true function f as well as an acquisition function which is a function of the posterior and guides the process of choosing the next sample point until a stopping criteria is met or the evaluation budget B is exhausted.

Gaussian Processes and the Surrogate Model We use a non-parametric Gaussian process as the surrogate model of f as GPs define a probability distribution over functions and for Gaussian likelihood models the posterior distribution is analytically tractable. Moreover, they maintain smoothness and uncertainty estimates to guide the exploration of new points as well as represent prior beliefs (Schulz et al., 2018). Following Williams & Rasmussen (2006), for inputs $\mathbf{y}, \mathbf{y}' \in \mathcal{Y}$, a GP is defined as $g(\mathbf{y}) \sim GP(\mu(\mathbf{y}), k(\mathbf{y}, \mathbf{y}'))$ where $\mu(\mathbf{y})$ is the mean and $k(\mathbf{y}, \mathbf{y}')$ is a kernel function given by $k(\mathbf{y}, \mathbf{y}') = \text{cov}(g(\mathbf{y}), g(\mathbf{y}'))$. For N data points $Y = [\mathbf{y}_1, \dots, \mathbf{y}_N]$, the induced prior probability density $g(Y) = [g(\mathbf{y}_1), \dots, g(\mathbf{y}_N)]^T$ is a multivariate Gaussian distribution: $g(Y) \sim \mathcal{N}(\mathbf{0}, K_{Y,Y})$. We assume $\mu(\mathbf{y}) \equiv 0$ throughout this work. The elements of the covariance

matrix are defined by the kernel function $[K_{Y,Y}]_{i,j} = k(\mathbf{y}_i, \mathbf{y}_j)$. GPs are intractable for large datasets as the time complexity scales by $\mathcal{O}(N^3)$. Several approximate methods have been proposed to address this through sparse Gaussian processes (Smola & Bartlett, 2000; Lawrence et al., 2002; Quinero-Candela & Rasmussen, 2005) or via (stochastic) variational formulations (Titsias, 2009; Hensman et al., 2013) for sparse approximations.

Acquisition Functions An acquisition function is a function of the posterior that captures the trade-off between exploration and exploitation of our surrogate of the function f given the known evaluations. It is responsible for selecting the next candidate point in \mathcal{Y} that should be evaluated or measured. We use an acquisition function $\alpha(\mathbf{y})$ to choose the next sample point $\mathbf{y}_{N+1} = \arg \max_{\mathbf{y}} \alpha(\mathbf{y})$. A good acquisition function exploits regions around the current maximum by selecting points to query from that region while also suggesting points from unexplored regions in order to escape a local maxima. There are several candidate functions such as upper confidence bound, expected improvement, probability of improvement, and Thompson sampling (Shahriari et al., 2015). Our proposed method is agnostic to the choice of acquisition function.

3.2 VARIATIONAL AUTOENCODERS

We define a latent variable generative model as $p_{\omega}(\mathbf{y}, \mathbf{z}) = p_{\psi}(\mathbf{y} | \mathbf{z})p_{\theta}(\mathbf{z})$ which is parameterised by $\omega = \{\psi, \theta\}$, and where \mathbf{z} is unobserved. We are generally interested in inferring this latent variable \mathbf{z} given \mathbf{y} . The posterior distribution, $p_{\omega}(\mathbf{z} | \mathbf{y}) = p_{\psi}(\mathbf{y} | \mathbf{z})p_{\theta}(\mathbf{z})/p_{\omega}(\mathbf{y})$, is usually intractable due to the lack of a closed-form marginalisation over the latent space (Murphy, 2023). The standard VAE model comprises the generative model (the probabilistic decoder) $p_{\psi}(\mathbf{y} | \mathbf{z})$ and an inference model (the probabilistic encoder) $q_{\phi}(\mathbf{z} | \mathbf{y})$ that approximates the true posterior. VAEs use amortised variational inference that exploits the inference model $q_{\phi}(\mathbf{z} | \mathbf{y})$ to obtain approximate distributions for each \mathbf{z}_n . The encoder and decoder are typically parameterised by deep neural networks. In variational inference we minimise the Kullback-Leibler (KL) divergence from $q_{\phi}(\mathbf{z} | \mathbf{y})$ to $p_{\omega}(\mathbf{z} | \mathbf{y})$, or equivalently maximise the ELBO of the marginal log-likelihood w.r.t. ϕ . For VAEs, approximate inference is typically conducted alongside learning the generative model’s parameters, that is, w.r.t. ϕ, ψ, θ :

$$\log p_{\omega}(Y) \geq \mathcal{L}(\phi, \psi, \theta; Y) \triangleq \sum_{n=1}^N \mathbb{E}_{q_{\phi}}[\log p_{\psi}(\mathbf{y}_n | \mathbf{z}_n)] - \text{KL}[q_{\phi}(\mathbf{z}_n | \mathbf{y}_n) || p_{\theta}(\mathbf{z}_n)] \rightarrow \max_{\phi, \psi, \theta}.$$

It is straightforward to apply computationally efficient mini-batch based stochastic gradient descent to the above equation.

4 OUR METHOD

4.1 BAYESIAN OPTIMISATION WITH VAES

The low-dimensional nonlinear latent manifold learnt by a VAE can be used to perform BO (Kusner et al., 2017; Gómez-Bombarelli et al., 2018; Tripp et al., 2020). The VAE is first pre-trained on the high-dimensional observations without access to the utility function values. As described in Sec. 3.2, the encoder $q_{\phi}(\mathbf{z} | \mathbf{y})$ of the learnt VAE is used to map the observations $\mathbf{y} \in \mathcal{Y}$ onto a low-dimensional latent representation $\mathbf{z} \in \mathcal{Z}$. The VAE-based methods then perform latent space optimisation (LSO) (Tripp et al., 2020) by fitting a surrogate model over the latent space to model the utility function of interest. The VAE BO aims to identify a \mathbf{z}^* such that the corresponding \mathbf{y}^* , that is obtained from the pre-trained decoder, minimises a utility function of interest, $f(\mathbf{y}^*)$. In other words, we would like to obtain a \mathbf{z}^* such that we maximise the expectation over the utility function evaluated on $\mathbf{y}^* \sim p_{\psi}(\mathbf{y}^* | \mathbf{z}^*)$, i.e., $\arg \max_{\mathbf{z} \in \mathcal{Z}} \mathbb{E}_{\mathbf{y} \sim p_{\psi}(\cdot | \mathbf{z})}[f(\mathbf{y})]$. Once we have a new \mathbf{y}^* and its associated utility function value c , we append them to the training dataset and update the parameters ϕ and ψ either after each BO step or at a chosen frequency. Tripp et al. (2020) use this approach with the help of a weighted retraining scheme according to their utility function values.

4.2 GAUSSIAN PROCESS PRIOR VAES FOR BO

A limitation of standard VAE BO is that it infers an unconditional latent-variable model without any guidance from the observed target quantities. Departures from this limitation have been proposed,

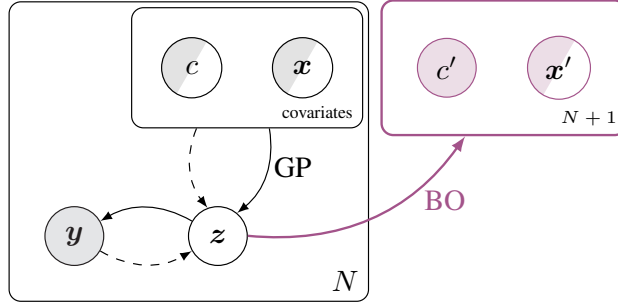
216
217
218
219
220
221
222
223
224
225
226

Figure 2: *Our proposed model.* Solid lines refer to the generative model and dashed lines to the inference model. Empty circles are unobserved, shaded circles are observed, and partially shaded circles are partially observed. Target quantity c' and possible additional covariates x' refer to the new candidate observation that will be added to the training set.

231
232
233
234
235
236

e.g., in (Eissman et al., 2018; Tripp et al., 2020; Maus et al., 2022). Recently, Grosnit et al. (2021) built upon VAE BOs by using deep metric learning to actively steer the generative model to maintain a latent manifold that is useful for the BO task. We propose to use GP prior VAEs that guide the generative model by conditioning the GP prior with auxiliary covariates.

237
238
239
240
241
242
243
244
245
246

The key distinction of GP prior VAEs is that the factorisable conditional prior defined over the latent space $p_\theta(Z|X) = \prod_{i=1}^N p_\theta(z_i | x_i)$ is replaced by a GP prior. Assuming a function $\tau : \mathcal{X} \rightarrow \mathcal{Z}$, which maps auxiliary covariates to the L -dimensional latent space, we denote $z = \tau(x) = (\tau_1(x), \dots, \tau_L(x))^T$. GP prior VAEs model each latent dimension with an independent GP $\tau_l(x) \sim \mathcal{GP}(\mu_l(x), k_l(x, x' | \theta_l))$, where $\mu_l(x)$ is the mean, $k_l(x, x' | \theta_l)$ is the covariance function, and θ_l denotes the parameters of the covariance function. The GP prior for the l^{th} latent dimension can be written as a joint multivariate Gaussian distribution for the function values $\bar{z}_l = \tau_l(X) = (\tau_l(x_1), \dots, \tau_l(x_N))^T$, such that $p_\theta(\bar{z}_l | X) = p_\theta(\tau_l(X)) = \mathcal{N}(\bar{z}_l | \mathbf{0}, K_{XX}^{(l)})$, where $\{K_{XX}^{(l)}\}_{i,j} = k_l(x_i, x_j | \theta_l)$. Our joint conditional prior is

247
248
249
250

$$p_\theta(Z | X) = \prod_{l=1}^L p_\theta(\bar{z}_l | X) = \prod_{l=1}^L \mathcal{N}(\bar{z}_l | \mathbf{0}, K_{XX}^{(l)}).$$

251
252
253
254
255
256
257
258
259
260
261
262
263

We propose to learn a low-dimensional latent embedding for BO using a GP prior VAE that is conditioned on the target quantity of interest, i.e., $p_\theta(Z | c)$. We hypothesise that using the target quantity as the conditioning variable will automatically guide the latent embeddings to a smooth manifold that is beneficial for the BO task. Since the target quantity $c \in \mathbb{R}$, the GP prior VAE can be defined using any of the commonly used smooth kernel functions, such as the squared exponential kernel. Following the same reasoning, if data points y have any additional known properties x , we can incorporate those in the GP prior VAE framework as well by conditioning the latent variable generation with both c and x (we denote $\tilde{x} = [c, x]$), i.e., $p_\theta(Z | \tilde{X})$. If all auxiliary covariates in \tilde{x} are continuous, we could incorporate \tilde{x} , e.g., via a single squared exponential kernel with a shared length-scale parameter or use an automatic relevance determination (ARD) kernel to define covariate-specific length-scales. In practice, however, some of the auxiliary covariates may be, e.g., binary or categorical. Ramchandran et al. (2021) have shown that it is possible to have flexible and expressive covariance functions depending on the nature of the auxiliary covariates. In this work, we similarly assume $Q + 1$ additive covariance functions,

264
265
266
267

$$k_l(\tilde{x}, \tilde{x}' | \theta_l) = k_l(c, c' | \theta_l) + \sum_{r=1}^Q k_{l,r}(x_r, x'_r | \theta_{l,r}) + \sigma_{z_l}^2,$$

268
269

implying that $K_{\tilde{X}\tilde{X}}^{(l)} = K_{cc}^{(l)} + \sum_{r=1}^Q K_{X_r X_r}^{(l,r)} + \sigma_{z_l}^2 I_N$, where the choice of the kernels depends on the application and X_r denotes the r^{th} auxiliary variable.

Algorithm 1: An overview of our proposed algorithm

Input: Budget B , frequency ν , initial dataset \mathcal{D} , pre-trained VAE

for $j = 1$ **to** $J \equiv \lceil B/\nu \rceil$ **do**

// **Train the GP prior VAE on** $\mathcal{D} = \mathcal{D}_0 \cup \mathcal{D}_U$

Solve $\phi_j^*, \psi_j^*, \theta_j^* \leftarrow \arg \max_{\phi, \psi, \theta} \text{ELBO}_{\text{GP-VAE-miss}}(\phi, \psi, \theta)[\mathcal{D}]$;

Compute $\mathcal{D}_Z \leftarrow \langle z_i, f(\mathbf{y}_i) \rangle_{i \in \mathcal{I}_0}$ by using the encoder ϕ_j^* to obtain z_i ;

for $k = 0$ **to** $\nu - 1$ **and** $EI(\hat{z}_{j,k+1}) \geq \eta$ **do** // **Perform Bayesian optimisation**

Fit surrogate GP on $\langle z_i, f(\mathbf{y}_i) \rangle_{i \in \mathcal{I}_0}$;

Optimise EI for $\hat{z}_{j,k+1}$;

Use decoder ψ_j^* to map $\hat{z}_{j,k+1}$ to $\hat{\mathbf{y}}$; // **Decode point chosen by B.O.**

Evaluate $c = f(\hat{\mathbf{y}})$, augment data $\mathcal{D}_0, \mathcal{D}_Z$; // **Evaluate black-box function**

Increment N^o ;

end

end

Output: $\mathbf{y}^* = \arg \max_{\mathbf{y} \in \mathcal{D}_0} f(\mathbf{y})$

4.3 PARTIALLY OBSERVED TARGET QUANTITY AND ADDITIONAL COVARIATES

In the BO setting, the target quantity of interest that we are optimising is typically available only for a (very) small number of data points. This is problematic for conditional generative models, such as GP prior VAEs, as they assume that covariates that are used to condition the generation are always known and observed. Moreover, in our problem setting, the additional auxiliary covariates that may be available in a specific application may also have missing values. We follow a formulation similar to that of Ramchandran et al. (2024) to handle the missing values in the covariates.

We augment our generative model with a prior distribution, $p_\lambda(\tilde{\mathbf{x}})$, factorising over $\tilde{\mathbf{x}}$, parameterised by λ . Representing the observed and unobserved parts as $Y = (Y^o, Y^u)$ and $\tilde{X} = (\tilde{X}^o, \tilde{X}^u)$, we approximate the true posterior distribution of the unobserved variables Z and \tilde{X}^u , represented as $p_\gamma(Z, \tilde{X}^u \mid Y^o, \tilde{X}^o)$ and parameterised by $\gamma = \{\psi, \theta, \lambda\}$, using amortised variational inference. We make use of a conditionally independent, factorisable variational approximation: $q_\phi(Z, \tilde{X}^u \mid Y^o, \tilde{X}^o) = q_\phi(Z \mid Y^o, \tilde{X}^o)q_\phi(\tilde{X}^u \mid \tilde{X}^o) = \prod_{i=1}^N q_\phi(z_i \mid \mathbf{y}_i^o, \tilde{\mathbf{x}}_i^o)q_\phi(\tilde{\mathbf{x}}_i^u \mid \tilde{\mathbf{x}}_i^o)$. The latent variables z_i are assumed to have a Gaussian variational distribution and, for the discrete and continuous-valued covariates $\tilde{\mathbf{x}}_i^u$, categorical and Gaussian distributions respectively. Following Ramchandran et al. (2024), we write the ELBO objective with missing covariates ($\text{ELBO}_{\text{GP-VAE-miss}}$) as

$$\begin{aligned} \log p_\gamma(Y^o \mid \tilde{X}^o) &\geq \mathbb{E}_{q_\phi}[\log p_\psi(Y^o \mid Z)] - \mathbb{E}_{q_\phi} \left[\text{KL}[q_\phi(Z \mid Y^o, \tilde{X}^o) \parallel p_\theta(Z \mid \tilde{X}^u, \tilde{X}^o)] \right] \\ &\quad - \text{KL}[q_\phi(\tilde{X}^u \mid \tilde{X}^o) \parallel p_\lambda(\tilde{X}^u \mid \tilde{X}^o)], \end{aligned} \quad (1)$$

where the first and the second expectations are with respect to the latent variables Z and missing covariates \tilde{X}^u , respectively, and can be approximated using Monte Carlo (see the Sec. A of the Appendices for details of deriving the ELBO). For each specific value of the missing covariates, the KL divergence in Eq. 1 has a computation complexity of $\mathcal{O}(N^3)$. Earlier work by Ramchandran et al. (2021; 2024) has shown that using the low-rank inducing point approximation for the multi-output GP $p_\theta(Z \mid \tilde{X}^u, \tilde{X}^o) = p_\theta(Z \mid X)$, one can derive a scalable ELBO that provides an unbiased, mini-batch compatible lower bound for efficient learning. See the Sec. A.1 of the Appendices for the specific expression of the scalable lower bound that we use.

4.4 HIGH-DIMENSIONAL BO WITH GAUSSIAN PROCESS PRIOR VAES

We use the latent space learnt by the GP prior VAE to perform efficient BO. In particular, our method can handle missing values in both the observations \mathbf{y} and covariates \mathbf{x} (partially observed features denoted as \mathbf{y}^o and \mathbf{x}^o), as well as large datasets through the scalable ELBO described in Sec. 4.3. Consider a dataset $\mathcal{D} = \mathcal{D}_0 \cup \mathcal{D}_U$ where \mathcal{D}_0 represents the data points whose target quantity c is observed (indexed by \mathcal{I}_0) and \mathcal{D}_U represents the data points whose c is unobserved (indexed by \mathcal{I}_U). Therefore, $\mathcal{D}_0 = \{\mathbf{y}_i^o, \mathbf{x}_i^o, c_i\}_{i \in \mathcal{I}_0}$, with $c_i = f(\mathbf{y}_i)$ and $\mathcal{D}_U = \{\mathbf{y}_i^o, \mathbf{x}_i^o\}_{i \in \mathcal{I}_U}$, where, as before,

$x_i \in \mathcal{X}$ refers to the additional auxiliary covariates (that may or may not be available, depending on the application), and $f(\cdot)$ refers to an expensive black-box function. N refers to the total number of observations, comprising the number of observations with observed quantity of interest $N^o = |\mathcal{I}_O|$ and number of observations with unobserved quantity of interest $N^u = |\mathcal{I}_U|$.

Algorithm See Algorithm 1 for a pseudo-code summary of our method. Budget B refers to the maximum number of evaluations of the black-box function that can be performed, ν refers to the number of BO steps performed before re-optimising our GP prior VAE model with the augmented dataset \mathcal{D} , and EI pertains to the expected improvement acquisition function (the algorithm is agnostic to this choice).

We obtain the optimal encoder and decoder parameters (ϕ_l^* and ψ_l^* respectively) by optimising the ELBO (in Sec. 4.3). The method computes the fully-observed, low-dimensional latent space representation z_i of the observations y_i^o using the optimal encoder at the current iteration, and implements a BO step. The new chosen observation \hat{y} , its covariates (if known), and the obtained target quantity of interest $c = f(\hat{y})$ are appended to \mathcal{D}_O . After budget has been exhausted, our algorithm returns the best candidate acquired so far.

5 EXPERIMENTS

We demonstrate the efficacy of our method described in Algorithm 1 on simulated datasets as well as on a molecular discovery benchmark dataset. In all our experiments, 10% of the training data is used as a held-out validation set for early-stopping to ensure that the generative model does not overfit. We describe the neural network architectures in the Sec. E of the Appendices. We use the same BO options and underlying VAE architectures for all methods in a particular experiment. We benchmark against the following methods:

LSO This latent space optimisation method uses a VAE to learn a low-dimensional representation of the high-dimensional dataset. BO is performed over the low-dimensional latent space. LSO does not take into account any auxiliary covariate information and makes use of a standard Gaussian prior over the latent space.

[Grosnit et al. \(2021\)](#) proposed a VAE-based method that tries to construct discriminative latent spaces for VAE-based BO methods by incorporating a metric loss term in the ELBO. We compare our model against the triplet loss, log-ratio loss, and contrastive loss.

Triplet Loss (T-LBO) As described in [Grosnit et al. \(2021\)](#), the triplet loss measures distances between input triplets. In other words, this loss tries to introduce a structured space where positive and negative pairs cluster together subject to separation by a margin. The triplet pairs are assigned as a pre-processing step.

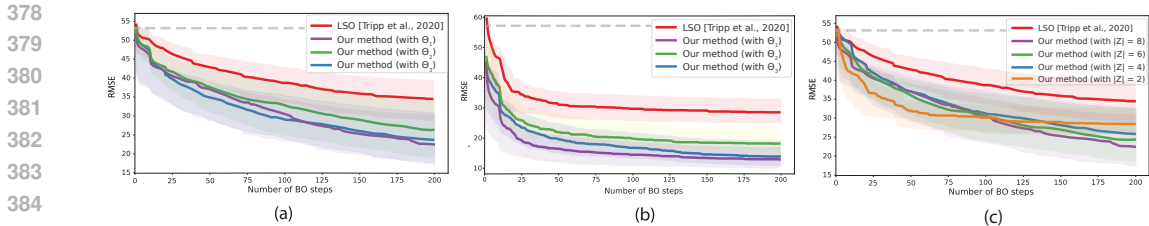
Log-Ratio Loss (LR-LBO) This metric loss is described in [Kim et al. \(2019\)](#) and is a continuous metric loss that is applied to triplets of inputs. This loss is used with the model described in [Grosnit et al. \(2021\)](#).

Contrastive Loss (C-LBO) This deep metric loss is described in [Hadsell et al. \(2006\)](#). The contrastive loss operates on input pairs by separating the latent encodings based on class label information. This is used with the model described in [Grosnit et al. \(2021\)](#).

Local Latent Bayesian Optimisation (LOL-BO) As proposed in [Maus et al. \(2022\)](#), this method is a latent space BO approach that addresses the mismatch between the notion of a trust region in the latent space and a trust region in the structured input space.

5.1 DEMONSTRATION ON SYNTHETIC DATA

We demonstrate our model’s ability to perform effective high-dimensional BO by modifying digits from the MNIST dataset. In particular, we randomly select an instance of a digit and resize this digit to a dimension of 52×52 pixels for a larger image space. We perform three different manipulations (which would form our additional auxiliary covariates x) to this digit: rotation about the centre, shift along the x -axis, and shift along the y -axis, by stochastically choosing these values 500 or 5000 times. Our final training set comprises either 500 or 5000 samples. Further-



378
 379
 380
 381
 382
 383
 384
 385
 386
 387
 388
 389
 390
 391
 392
 393
 394
 395
 396
 397
 398
 399
 400
 401
 402
 403
 404
 405
 406
 407
 408
 409
 410
 411
 412
 413
 414
 415
 416
 417
 418
 419
 420
 421
 422
 423
 424
 425
 426
 427
 428
 429
 430
 431

Figure 3: Results from our experiments with a synthetic dataset. **Lower values are better.** (a) Comparing the performance of our model with the LSO benchmark. The dataset comprises 500 instances out of which the target quantity is observed only for 100 instances. Θ_1 pertains to an additive GP prior VAE over all three covariates \mathbf{x} and the partially observed quantity of interest c , Θ_2 to a GP prior VAE over only the partially observed target c , and Θ_3 to an additive GP prior VAE over the partially observed quantity of interest c and shift $_{\mathbf{x}}$. (b) Similarly, we also demonstrate our model’s performance on a dataset which comprises 5000 instances out of which the quantity of interest is observed only for 500 instances. (c) Effect of the choice of latent dimension with the dataset comprising 500 instances. $|Z|$ pertains to the dimensionality of the latent space. All plots depict the mean quantity of interest value with the 95% confidence interval (shaded region) obtained over 100 repetitions with regenerated training data and target images. The grey line pertains to the lowest RMSE in the training set.

more, we define a ‘target image’, $\mathbf{y}^{\text{target}}$, with a particular rotation and shift values. This target image is not included in the training set and we ensure that the manipulations are sufficiently different from the target values. See Suppl. Fig. 7 for a random sample of the training data. In this experiment, the black-box function is the root mean squared error (RMSE) between the unseen target digit and a chosen digit (either a digit from the training set or a new candidate), i.e., $f(\mathbf{y}) = \text{RMSE}(\mathbf{y}^{\text{target}} - \mathbf{y})$. Our objective is to find a new digit that minimises the value returned by the black-box function. In other words, we want the quantity of interest to be as close to zero as possible. Furthermore, in our training set, we assume that the quantity of interest $c = f(\mathbf{y})$ (i.e. the RMSE between the unseen target and the digit) is known for only a few digits (i.e., $|\mathcal{I}_0|$ equals 100 or 500) and unobserved for the rest.

To ensure that there is sufficient stochasticity in the choice of targets, we repeat our experiments as well as the generation of data 100 times. We fit our GP prior VAE-based method by making use of the partially observed target quantity of interest c as well as (a subset of) the auxiliary covariates \mathbf{x} . We make use of Algorithm 1 with $\nu = 10$ as well as $B = 200$. We experiment with different choices of kernels to empirically obtain the optimal model.

Fig. 3 demonstrates our experiments on the synthetic dataset and we can see that our method finds candidate points with a quantity of interest (or RMSE) that are significantly lower than those in the training set. In Fig. 3(a) we demonstrate the performance of our model on 500 instances out of which the quantity of interest is observed for 100 instances. The LSO method is trained with all 500 instances and the BO computation is performed using the 100 instances for which the quantity of interest is observed. Our method outperforms the

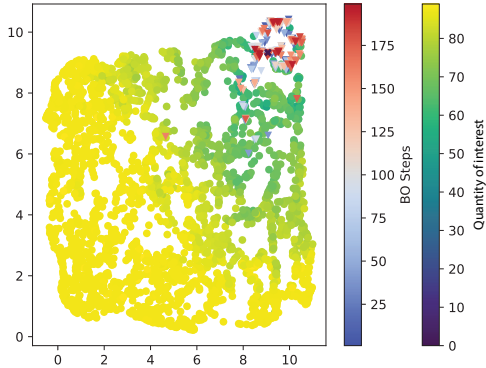


Figure 4: Visualisation of the latent space in the synthetic data experiment. We performed a projection of the latent space down to two dimensions using UMAP. The inverted triangles refer to the BO steps and the blue cross refers to the latent space representation of the ‘optimal’ instance which we hope our method would find (not included in the training set). The latent embedding is coloured by the quantity of interest.

432 LSO model already when the GP prior VAE is fitted with the partially observed target quantity (Θ_2),
433 and results improves further if additional auxiliary covariates are available (Θ_1 and Θ_3).

434 Similarly, Fig. 3(b) demonstrates that our method outperforms the baseline LSO with 5000 instances
435 out of which the quantity of interest is observed for 500 instances and Fig. 3(c) demonstrates the
436 effect of the choice of latent dimension.
437

438 We visualise the learnt latent space and the BO steps taken in Fig. 4. Our method learns latent
439 representations where the target quantity increases smoothly from the lower left corner to the upper
440 right corner (though we again emphasise that this is a 2-D UMAP visualisation). The BO steps
441 explore the region of the latent space where the target quantity has high values. In Suppl. Fig. 6, we
442 perform ablations with different subsets of additional auxiliary covariates.

443 5.2 EXPRESSION RECONSTRUCTION

444 We consider the common task of generating single-variable mathematical expressions from a formal
445 grammar (Kusner et al., 2017; Tripp et al., 2020; Grosnit et al., 2021; Maus et al., 2022). The objective
446 is to minimise a distance/regret based on mean squared error (MSE) (defined as $\log(1 + \text{MSE})$)
447 between a generated expression and the target expression, $x * \sin(x * x)$. We followed the data
448 preparation proposed by Grosnit et al. (2021) to obtain 40000 data points and augmented the data
449 with 8 additional covariates (count of the elements ‘/’, ‘*’, ‘+’, ‘exp’, ‘sine’, ‘1’, ‘2’, and ‘3’ in the
450 expressions) which can be easily gleaned from the expressions. In order to appropriately handle
451 the mathematical expressions, we use the Grammar VAE (Kusner et al., 2017). To demonstrate the
452 efficacy of our method, we make use of Algorithm 1 with $\nu = 10$ and $B = 500$ as well as an additive
453 kernel over the 8 additional covariates and regret. Fig. 5(a) demonstrates that our method achieves
454 competitive performance against the benchmark methods. In Suppl. Fig. 10, we visualise the mean
455 regret achieved by our method together with the 95% confidence interval.
456

457 5.3 MOLECULE OPTIMISATION

458 We use the ZINC-250K molecular dataset used in Gómez-Bombarelli et al. (2018), which consists
459 of 250000 drug-like commercially available molecules extracted from the ZINC database (Irwin
460 et al., 2012) - a public dataset for ligand discovery. The dataset includes the molecular structures
461 in the SMILES string representation (Weininger, 1988) and three molecular properties: the water-
462 octanol partition coefficient (logP), the Synthetic Accessibility Score (SAS), and the Quantitative
463 Estimation of Drug-likeness (QED). The objective of the task is to maximise the penalised logP which
464 is defined as the logP penalised by the SAS and the number of long cycles: $\text{penalised logP}(m) =$
465 $\text{logP}(m) - \text{SAS}(m) - \text{cycle}(m)$ where m is the molecular instance and $\text{cycle}(\cdot)$ is the number of
466 long cycles.
467

468 We augmented the ZINC-250K with five additional covariates: molecular weight, number of hydrogen
469 donors, number of hydrogen acceptors, number of rotatable bonds, and total polar surface area. These
470 values were computed using a popular open-source chem-informatics tool, RDKit (Landrum et al.,
471 2013) (see Suppl. Fig. 11 for a visualisation of the distribution of these properties in the form
472 of histograms). Including QED and SAS, there are seven additional auxiliary covariates and the
473 penalised logP is the quantity of interest which we are trying to maximise. For a new molecule, it is
474 possible to compute the penalised logP using RDKit (acting as our black-box function). Furthermore,
475 we assume that the penalised logP is partially observed (observed for only 1% of the data).

476 We demonstrate the ability of our model to optimise the structure of the molecule in order to maximise
477 a property of interest (the penalised logP). To handle the SMILES representation of the molecules,
478 we use the Junction Tree VAE (JT-VAE) (Jin et al., 2018), which introduced an encoder and decoder
479 suitable to molecular graphs. In our experiments, we extend the implementation by Grosnit et al.
480 (2021). We note that our method is not limited to JT-VAE but can be applied with any latent-variable
481 model. Furthermore, we use JT-VAE with all the baseline methods for a fair comparison.

482 We use Algorithm 1 with $\nu = 10$ and $B = 450$. In Fig. 5(b) we demonstrate that our method is able
483 to identify candidate molecules that have a higher penalised logP value than competing methods.
484 Furthermore, in Fig. 5(c), we demonstrate the performance of our method with different choices
485 of auxiliary covariates for the additive kernel of the GP prior. The results show that it is indeed
beneficial to include the additional auxiliary covariate information, whenever they are available in an

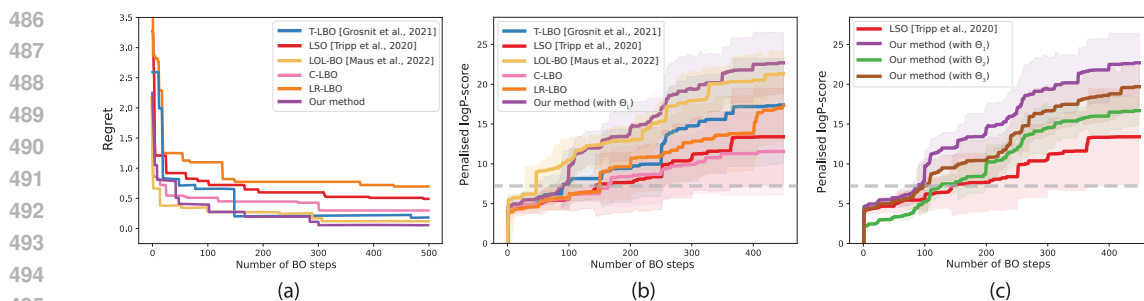


Figure 5: Results from the expression reconstruction and molecule optimisation experiments. (a) The mean regret achieved over 5 repetitions. **Lower values are better**. (b) The penalised logP score achieved by our method compared to competing methods. (c) Comparison of the penalised logP score achieved by our method using different choices of additional covariates in the additive kernel of the GP prior VAE. Θ_1 pertains to an additive kernel over all 7 covariates and the partially observed target quantity, Θ_2 to a kernel over only the partially observed target quantity, and Θ_3 to an additive kernel over only the 5 additional properties that were calculated with RDKit (and does not include the partially observed target quantity). In figures (b) and (c), the mean penalised logP score over 10 repetitions is visualised together with the 95% confidence interval (shaded region). The grey line pertains to the highest penalised logP score in the training set. **Higher values are better**

application, along with the partially observed quantity of interest (penalised logP). See Suppl. Fig. 12 for a visualisation of the marginal variance of the additive components. We visualise the mean and standard deviation of the marginal variance for each of the kernel components across the 56 latent dimensions. In Suppl. Fig. 13, we demonstrate the performance of our method with fewer instances for which the penalised logP is observed. For this experiment, we assumed that the penalised $\log P$ is observed for only 0.1% of the data. The overall performance of all the methods decreases because the BO has fewer points to fit the surrogate model with. However, it is interesting to note that our method with an additive kernel that does not include the quantity of interest performs the best. We postulate that this is because only a few instances of the quantity of interest are observed and hence the estimated values for the unobserved quantities of interest have low quality. We believe that this demonstrates that our model is able to learn meaningful latent representations without making use of the partially observed quantity of interest and can be applied to datasets with only a few labelled instances.

In Suppl. Fig 14, we visualise the latent space using t-SNE and colour the latent embedding by the respective molecular properties. We note that the model learns a latent embedding that changes smoothly with respect to the target quantity as well as with the respect to the additional covariates.

6 CONCLUSION

In this paper, we proposed a novel GP prior VAE-based method to perform high-dimensional BO. We demonstrated the efficacy of our method on simulated datasets as well as in the discovery of novel molecules that optimise a quantity of interest. Our method shows that it can be beneficial to include auxiliary covariates (even partially observed) for performing BO in the latent space. Furthermore, our approach can efficiently handle partially observed target quantities. Given the flexibility and performance of our model, we expect our approach to be beneficial to scalable BO.

REFERENCES

- Mickael Binois and Nathan Wycoff. A survey on high-dimensional gaussian process modeling with application to bayesian optimization. *ACM Transactions on Evolutionary Learning and Optimization*, 2(2):1–26, 2022.
- Francesco Paolo Casale, Adrian Dalca, Luca Saglietti, Jennifer Listgarten, and Nicolo Fusi. Gaussian process prior variational autoencoders. In *Advances in Neural Information Processing Systems*, 2018.

- 540 Stephan Eissman, Daniel Levy, Rui Shu, Stefan Bartzsch, and Stefano Ermon. Bayesian optimization
541 and attribute adjustment. In *Proceedings of the 34th Conference on Uncertainty in Artificial*
542 *Intelligence*, 2018.
- 543
- 544 Kobi Felton, Daniel Wigh, and Alexei Lapkin. Multi-task bayesian optimization of chemical reactions.
545 In *Machine Learning for Molecules Workshop at NeurIPS*, 2020.
- 546
- 547 Vincent Fortuin, Dmitry Baranchuk, Gunnar Rätsch, and Stephan Mandt. Gp-vae: Deep probabilistic
548 time series imputation. In *International conference on artificial intelligence and statistics*, pp.
1651–1661. PMLR, 2020.
- 549
- 550 Peter I Frazier. Bayesian optimization. In *Recent advances in optimization and modeling of*
551 *contemporary problems*, pp. 255–278. Informs, 2018.
- 552
- 553 Rafael Gómez-Bombarelli, Jennifer N Wei, David Duvenaud, José Miguel Hernández-Lobato,
554 Benjamín Sánchez-Lengeling, Dennis Sheberla, Jorge Aguilera-Iparraguirre, Timothy D Hirzel,
555 Ryan P Adams, and Alán Aspuru-Guzik. Automatic chemical design using a data-driven continuous
556 representation of molecules. *ACS central science*, 4(2):268–276, 2018.
- 557
- 558 Ryan-Rhys Griffiths and José Miguel Hernández-Lobato. Constrained bayesian optimization for
559 automatic chemical design using variational autoencoders. *Chemical science*, 11(2):577–586,
2020.
- 560
- 561 Antoine Grosnit, Rasul Tutunov, Alexandre Max Maraval, Ryan-Rhys Griffiths, Alexander I Cowen-
562 Rivers, Lin Yang, Lin Zhu, Wenlong Lyu, Zhitang Chen, Jun Wang, et al. High-dimensional
563 bayesian optimisation with variational autoencoders and deep metric learning. *arXiv preprint*
564 *arXiv:2106.03609*, 2021.
- 565
- 566 Raia Hadsell, Sumit Chopra, and Yann LeCun. Dimensionality reduction by learning an invariant
567 mapping. In *IEEE Computer Society Conference on Computer Vision and Pattern Recognition*
(*CVPR’06*), volume 2, pp. 1735–1742. IEEE, 2006.
- 568
- 569 James Hensman, Nicolo Fusi, and Neil D Lawrence. Gaussian processes for big data. In *Proceedings*
570 *of the 29th Conference on Uncertainty and Artificial Intelligence*, 2013.
- 571
- 572 Irina Higgins, Loic Matthey, Arka Pal, Christopher Burgess, Xavier Glorot, Matthew Botvinick,
573 Shakir Mohamed, and Alexander Lerchner. β -VAE: Learning basic visual concepts with a
constrained variational framework. In *International conference on learning representations*, 2017.
- 574
- 575 John J Irwin, Teague Sterling, Michael M Mysinger, Erin S Bolstad, and Ryan G Coleman. Zinc: a
576 free tool to discover chemistry for biology. *Journal of chemical information and modeling*, 52(7):
1757–1768, 2012.
- 577
- 578 Wengong Jin, Regina Barzilay, and Tommi Jaakkola. Junction tree variational autoencoder for
579 molecular graph generation. In *International Conference on Machine Learning*, pp. 2323–2332.
580 PMLR, 2018.
- 581
- 582 Kirthevasan Kandasamy, Willie Neiswanger, Jeff Schneider, Barnabas Poczos, and Eric P Xing.
583 Neural architecture search with bayesian optimisation and optimal transport. *Advances in Neural*
584 *Information Processing Systems*, 31, 2018.
- 585
- 586 Sungeon Kim, Minkyoo Seo, Ivan Laptev, Minsu Cho, and Suha Kwak. Deep metric learning beyond
587 binary supervision. In *Proceedings of the IEEE/CVF Conference on Computer Vision and Pattern*
Recognition, pp. 2288–2297, 2019.
- 588
- 589 Diederik P. Kingma and Max Welling. Auto-encoding variational bayes. In *2nd International*
590 *Conference on Learning Representations, ICLR*, 2014.
- 591
- 592 Ksenia Korovina, Sailun Xu, Kirthevasan Kandasamy, Willie Neiswanger, Barnabas Poczos, Jeff
593 Schneider, and Eric Xing. Chemo: Bayesian optimization of small organic molecules with syn-
thesizable recommendations. In *International Conference on Artificial Intelligence and Statistics*,
pp. 3393–3403. PMLR, 2020.

- 594 Matt J Kusner, Brooks Paige, and José Miguel Hernández-Lobato. Grammar variational autoencoder.
595 In *International Conference on Machine Learning*, pp. 1945–1954. PMLR, 2017.
- 596
597 Greg Landrum et al. Rdkit: A software suite for cheminformatics, computational chemistry, and
598 predictive modeling. *Greg Landrum*, 8, 2013.
- 599
600 Neil Lawrence, Matthias Seeger, and Ralf Herbrich. Fast sparse gaussian process methods: The
601 informative vector machine. *Advances in Neural Information Processing Systems*, 15, 2002.
- 602
603 Xiaoyu Lu, Javier Gonzalez, Zhenwen Dai, and Neil D Lawrence. Structured variationally auto-
604 encoded optimization. In *International Conference on Machine Learning*, pp. 3267–3275. PMLR,
2018.
- 605
606 Pierre-Alexandre Mattei and Jes Frellsen. Miwae: Deep generative modelling and imputation of
607 incomplete data sets. In *International Conference on Machine Learning*, pp. 4413–4423. PMLR,
2019.
- 608
609 Natalie Maus, Haydn T Jones, Juston S Moore, Matt J Kusner, John Bradshaw, and Jacob R Gardner.
610 Local latent space bayesian optimization over structured inputs. *Advances in Neural Information
611 Processing Systems*, 2022.
- 612
613 Jonas Mockus. *The Bayesian approach to local optimization*. Springer, 1989.
- 614
615 Riccardo Moriconi, Marc Peter Deisenroth, and KS Sesh Kumar. High-dimensional bayesian
616 optimization using low-dimensional feature spaces. *Machine Learning*, 109(9):1925–1943, 2020.
- 617
618 Kevin P Murphy. *Probabilistic machine learning: Advanced topics*. MIT Press, 2023.
- 619
620 Alfredo Nazabal, Pablo M Olmos, Zoubin Ghahramani, and Isabel Valera. Handling incomplete
621 heterogeneous data using vaes. *Pattern Recognition*, 107:107501, 2020.
- 622
623 Joaquin Quinero-Candela and Carl Edward Rasmussen. A unifying view of sparse approximate
624 gaussian process regression. *The Journal of Machine Learning Research*, 6:1939–1959, 2005.
- 625
626 Siddharth Ramchandran, Gleb Tikhonov, Kalle Kujanpää, Miika Koskinen, and Harri Lähdesmäki.
627 Longitudinal variational autoencoder. In *International Conference on Artificial Intelligence and
628 Statistics*, pp. 3898–3906. PMLR, 2021.
- 629
630 Siddharth Ramchandran, Gleb Tikhonov, Otto Lönnroth, Pekka Tiikkainen, and Harri Lähdesmäki.
631 Learning conditional variational autoencoders with missing covariates. *Pattern Recognition*, 147:
632 110113, 2024.
- 633
634 Danilo Jimenez Rezende, Shakir Mohamed, and Daan Wierstra. Stochastic backpropagation and
635 approximate inference in deep generative models. In *International Conference on Machine
636 Learning*, pp. 1278–1286. PMLR, 2014.
- 637
638 Binxin Ru, Xingchen Wan, Xiaowen Dong, and Michael Osborne. Interpretable neural architecture
639 search via bayesian optimisation with weisfeiler-lehman kernels. In *International Conference on
640 Learning Representations*, 2021.
- 641
642 Eric Schulz, Maarten Speekenbrink, and Andreas Krause. A tutorial on gaussian process regression:
643 Modelling, exploring, and exploiting functions. *Journal of Mathematical Psychology*, 85:1–16,
644 2018.
- 645
646 Bobak Shahriari, Kevin Swersky, Ziyu Wang, Ryan P Adams, and Nando De Freitas. Taking the
647 human out of the loop: A review of bayesian optimization. *Proceedings of the IEEE*, 104(1):
148–175, 2015.
- 648
649 Benjamin J Shields, Jason Stevens, Jun Li, Marvin Parasram, Farhan Damani, Jesus I Martinez
650 Alvarado, Jacob M Janey, Ryan P Adams, and Abigail G Doyle. Bayesian reaction optimization as
651 a tool for chemical synthesis. *Nature*, 590(7844):89–96, 2021.
- 652
653 Eero Siivola, Andrei Paleyes, Javier González, and Aki Vehtari. Good practices for bayesian
654 optimization of high dimensional structured spaces. *Applied AI Letters*, 2(2):e24, 2021.

648 Alex Smola and Peter Bartlett. Sparse greedy gaussian process regression. *Advances in Neural*
649 *Information Processing Systems*, 13, 2000.
650

651 Kihyuk Sohn, Honglak Lee, and Xinchen Yan. Learning structured output representation using deep
652 conditional generative models. *Advances in Neural Information Processing Systems*, 28, 2015.

653 Samuel Stanton, Wesley Maddox, Nate Gruver, Phillip Maffettone, Emily Delaney, Peyton Greenside,
654 and Andrew Gordon Wilson. Accelerating bayesian optimization for biological sequence design
655 with denoising autoencoders. In *International Conference on Machine Learning*, pp. 20459–20478.
656 PMLR, 2022.

657 Michalis Titsias. Variational learning of inducing variables in sparse gaussian processes. In *Artificial*
658 *Intelligence and statistics*, pp. 567–574. PMLR, 2009.
659

660 Austin Tripp, Erik Daxberger, and José Miguel Hernández-Lobato. Sample-efficient optimization in
661 the latent space of deep generative models via weighted retraining. *Advances in Neural Information*
662 *Processing Systems*, 33:11259–11272, 2020.

663 Raquel Urtasun and Trevor Darrell. Discriminative gaussian process latent variable model for
664 classification. In *Proceedings of the 24th International Conference on Machine Learning*, pp.
665 927–934, 2007.
666

667 David Weininger. SMILES, a chemical language and information system. 1. introduction to methodo-
668 logy and encoding rules. *Journal of Chemical Information and Computer Sciences*, 28(1):31–36,
669 1988.

670 Christopher KI Williams and Carl Edward Rasmussen. *Gaussian processes for machine learning*,
671 volume 2. MIT press Cambridge, MA, 2006.
672
673
674
675
676
677
678
679
680
681
682
683
684
685
686
687
688
689
690
691
692
693
694
695
696
697
698
699
700
701

702 Appendices

703 A DERIVATION OF THE ELBO

704 Following (Kingma & Welling, 2014), the ELBO of the marginal log-likelihood for the standard VAE
705 model can be written as:

$$706 \log p_\omega(Y) \geq \mathcal{L}(\phi, \psi, \theta; Y) \triangleq \sum_{n=1}^N \mathbb{E}_{q_\phi}[\log p_\psi(\mathbf{y}_n | \mathbf{z}_n)] - \text{KL}[q_\phi(\mathbf{z}_n | \mathbf{y}_n) || p_\theta(\mathbf{z}_n)] \rightarrow \max_{\phi, \psi, \theta}, \quad (2)$$

707 where ϕ and ψ are the encoder and decoder weights respectively, \mathbf{z} refers to the low-dimensional
708 latent representation, \mathbf{y} refers to the observations, and KL refers to the Kullback-Leibler divergence.

709 Since we use GP prior VAEs that assume independent priors for each of the latent dimensions, we
710 write the joint conditional prior as:

$$711 p_\theta(Z | X) = \prod_{l=1}^L p_\theta(\bar{\mathbf{z}}_l | X) = \prod_{l=1}^L \mathcal{N}\left(\bar{\mathbf{z}}_l | \mathbf{0}, K_{XX}^{(l)}\right),$$

712 where $\bar{\mathbf{z}}_l = \tau_l(X) = (\tau_l(\mathbf{x}_1), \dots, \tau_l(\mathbf{x}_N))^T$, $\tau_l(\mathbf{x}) \sim \mathcal{GP}(\mu_l(\mathbf{x}), k_l(\mathbf{x}, \mathbf{x}' | \theta_l))$ such that $\mu_l(\mathbf{x})$ is
713 the mean, $k_l(\mathbf{x}, \mathbf{x}' | \theta_l)$ is the covariance function and θ_l denotes the parameters of the covariance
714 function, and $K_{XX}^{(l)}$ is a $N \times N$ covariance matrix for the l^{th} latent dimension.

715 We summarise the observed and unobserved parts as $Y = (Y^\circ, Y^u)$ and $\tilde{X} = (\tilde{X}^\circ, \tilde{X}^u)$ and write
716 the ELBO as:

$$717 \log p_\gamma(Y^\circ | \tilde{X}^\circ) \geq \underbrace{\mathbb{E}_q[\log p_\psi(Y^\circ | Z)] - \text{KL}[q_\phi(Z, \tilde{X}^u | Y^\circ, \tilde{X}^\circ) || p_{\theta, \lambda}(Z, \tilde{X}^u | \tilde{X}^\circ)]}_{\triangleq \mathcal{L}(\phi, \psi, \theta, \lambda; Y^\circ, \tilde{X}^\circ)}. \quad (3)$$

718 We use a conditionally independent factorisable variational approximation:

$$719 q_\phi(Z, \tilde{X}^u | Y^\circ, \tilde{X}^\circ) = q_\phi(Z | Y^\circ, \tilde{X}^\circ) q_\phi(\tilde{X}^u | \tilde{X}^\circ) = \prod_{i=1}^N q_\phi(\mathbf{z}_i | \mathbf{y}_i^\circ, \tilde{\mathbf{x}}_i^\circ) q_\phi(\tilde{\mathbf{x}}_i^u | \tilde{\mathbf{x}}_i^\circ). \quad (4)$$

720 We assume that $q_\phi(\mathbf{z}_i | \mathbf{y}_i^\circ, \tilde{\mathbf{x}}_i^\circ)$ factorises also across the latent dimensions, which allows us to write
721 the variational approximation alternatively as

$$722 q_\phi(Z, \tilde{X}^u | Y^\circ, \tilde{X}^\circ) = q_\phi(Z | Y^\circ, \tilde{X}^\circ) q_\phi(\tilde{X}^u | \tilde{X}^\circ) = \prod_{l=1}^L q_\phi(\bar{\mathbf{z}}_l | Y^\circ, \tilde{X}^\circ) \prod_{i=1}^N q_\phi(\tilde{\mathbf{x}}_i^u | \tilde{\mathbf{x}}_i^\circ). \quad (5)$$

723 Following Ramchandran et al. (2024), we simplify the KL term in Eq. 3 as:

$$724 \begin{aligned} & \text{KL}[q_\phi(Z, \tilde{X}^u | Y^\circ, \tilde{X}^\circ) || p_{\theta, \lambda}(Z, \tilde{X}^u | \tilde{X}^\circ)] \\ &= \mathbb{E}_{q_\phi} \left[\text{KL}[q_\phi(Z | Y^\circ, \tilde{X}^\circ) || p_\theta(Z | \tilde{X}^u, \tilde{X}^\circ)] \right] + \text{KL}[q_\phi(\tilde{X}^u | \tilde{X}^\circ) || p_\lambda(\tilde{X}^u | \tilde{X}^\circ)] \\ &= \sum_{l=1}^L \underbrace{\mathbb{E}_{q_\phi} \left[\text{KL}[q_\phi(\bar{\mathbf{z}}_l | Y^\circ, \tilde{X}^\circ) || p_\theta(\bar{\mathbf{z}}_l | \tilde{X}^u, \tilde{X}^\circ)] \right]}_{\leq D_{\text{KL}}^1} + \sum_{i=1}^N \underbrace{\text{KL}[q_\phi(\tilde{\mathbf{x}}_i^u | \tilde{\mathbf{x}}_i^\circ) || p_\lambda(\tilde{\mathbf{x}}_i^u | \tilde{\mathbf{x}}_i^\circ)]}_{D_{\text{KL}}^2} \end{aligned} \quad (6)$$

725 by using the assumption of a factorising latent space, $p_\theta(Z | \tilde{X}^u, \tilde{X}^\circ) = \prod_{l=1}^L p_\theta(\bar{\mathbf{z}}_l | \tilde{X}^u, \tilde{X}^\circ)$
726 and a mean-field normal posterior for $q_\phi(\bar{\mathbf{z}}_l | Y^\circ, \tilde{X}^\circ)$, with a variational
727 mean $\bar{\boldsymbol{\mu}}_l = (\mu_{\phi, l}(\tilde{\mathbf{x}}_1^\circ, \mathbf{y}_1^\circ), \dots, \mu_{\phi, l}(\tilde{\mathbf{x}}_N^\circ, \mathbf{y}_N^\circ))^T$ and a covariance matrix
728 $W_l = \text{diag}(\sigma_{\phi, l}^2(\tilde{\mathbf{x}}_1^\circ, \mathbf{y}_1^\circ), \dots, \sigma_{\phi, l}^2(\tilde{\mathbf{x}}_N^\circ, \mathbf{y}_N^\circ))$ for the l^{th} latent dimension. The expectation in
729 Eq. 6 is w.r.t. the unobserved auxiliary covariates \tilde{X}^u that are the inputs to the GP kernel and,
730 therefore, the expectation does not have a closed form but can be approximated by Monte Carlo
731 sampling.

732 There are several different approaches to approximate the GP prior in order for the ELBO in Eq. 6 to
733 scale to large datasets. We make use of a mini-batch compatible approach proposed by Ramchandran
734 et al. (2021) that uses the inducing point method (Titsias, 2009; Hensman et al., 2013) and exploits
735 the structure of the GP prior, as described in the next section.

A.1 SCALABLE COMPUTATION AND MINIBATCHING

Each of the KL divergences $\text{KL}[q_\phi(\tilde{\mathbf{z}}_l|Y^\circ, \tilde{X}^\circ)||p_\theta(\tilde{\mathbf{z}}_l|\tilde{X}^u, \tilde{X}^\circ)]$ in Eq. 6 has a computation complexity of $\mathcal{O}(N^3)$. Below we drop the index of the latent dimension, l , for simplicity. Relying on the derivation proposed by Ramchandran et al. (2021) to obtain a scalable ELBO, we use the low-rank inducing point approximation for GPs and use M inducing locations $S = (\mathbf{s}_1, \dots, \mathbf{s}_M)$ in \mathcal{X} and the corresponding inducing function values $\mathbf{u}_l = (\tau_l(\mathbf{s}_1), \dots, \tau_l(\mathbf{s}_M))^T = (u_{l1}, \dots, u_{lM})^T$ for each latent dimension (Hensman et al., 2013). We explicitly keep track of the distribution of the Gaussian inducing values $\mathbf{u}_l \sim \mathcal{N}(\mathbf{m}_l, H_l)$, where \mathbf{m}_l and H_l are global variational parameters. We can then derive an upper-bound for the KL divergence $\text{KL}[\mathcal{N}(\tilde{\boldsymbol{\mu}}, W)||\mathcal{N}(\mathbf{0}, K_{\tilde{X}\tilde{X}})] \leq D_{\text{KL}}^1$ as well as an unbiased, batch-normalised partial sum over a subset of indices, $\mathcal{I} \subset \{1, \dots, N\}$ of size $|\mathcal{I}| = \hat{N}$ such that $\hat{D}_{\text{KL}}^1 \approx D_{\text{KL}}^1$, where

$$\begin{aligned} \hat{D}_{\text{KL}}^1 = & \frac{1}{2} \frac{N}{\hat{N}} \sum_{i \in \mathcal{I}} \left(\sigma_z^{-2} (K_{\tilde{\mathbf{x}}_i S} K_{SS}^{-1} \mathbf{m} - \tilde{\boldsymbol{\mu}}_i)^2 + \sigma_z^{-2} \sigma_i^2 + \sigma_z^{-2} \tilde{K}_{ii} \right. \\ & \left. + \sigma_z^{-2} \text{tr} \left((K_{SS}^{-1} H K_{SS}^{-1}) (K_{S\tilde{\mathbf{x}}_i} K_{\tilde{\mathbf{x}}_i S}) \right) - \log \sigma_i^2 \right) + \frac{N}{2} \log \sigma_z^2 - \frac{N}{2} \\ & + \text{KL}[\mathcal{N}(\mathbf{m}, H)||\mathcal{N}(\mathbf{0}, K_{SS})], \end{aligned} \quad (7)$$

where $\tilde{\boldsymbol{\mu}}_i = \tilde{\boldsymbol{\mu}}_\phi(\tilde{\mathbf{x}}_i, \mathbf{y}_i^\circ)$ and $\sigma_i^2 = \sigma_\phi^2(\tilde{\mathbf{x}}_i, \mathbf{y}_i^\circ)$ are the encoder means and variances, \tilde{K}_{ii} denotes the i^{th} diagonal element of $\tilde{K} = K_{\tilde{X}\tilde{X}} - K_{\tilde{X}S} K_{SS}^{-1} K_{S\tilde{X}}$, and K_{SS} as well as $K_{\tilde{\mathbf{x}}_i S} = K_{S\tilde{\mathbf{x}}_i}^T$ are defined similarly as $K_{\tilde{X}\tilde{X}}$. The conditional probability $p_\lambda(\tilde{X}^u|\tilde{X}^\circ)$ in Eq. 6 simplifies to $p_\lambda(\tilde{X}^u|\tilde{X}^\circ) = p_\lambda(\tilde{X}^u)$. As described in (Ramchandran et al., 2024), $p_\lambda(\tilde{X}^u)$ can be an informative prior and D_{KL}^2 is amenable to mini-batching.

Therefore, the ELBO for GP prior VAE models that marginalises missing covariates and affords efficient optimisation with stochastic gradient descent is obtained from the Eqs. 3, 6, 7. For a more detailed derivation, please refer to Ramchandran et al. (2021; 2024).

B THE EXPECTED IMPROVEMENT ACQUISITION FUNCTION

The expected improvement acquisition function estimates improvement that would be achieved when choosing a specific point \mathbf{z} as the next point to query. It balances between exploration and exploitation of the black-box function f . The expected improvement (EI) is defined as

$$\alpha(\mathbf{z}) = \text{EI}(\mathbf{z}) = \int_{-\infty}^{\infty} \underbrace{\max(f(\mathbf{z}) - f^*, 0)}_{\text{Improvement}} \varphi\left(\frac{f(\mathbf{z}) - \mu(\mathbf{z})}{\sigma(\mathbf{z})}\right) df(\mathbf{z}),$$

where f^* is our current optimum, \mathbf{y} is an instance in the data space, $\hat{\mathbf{y}} \leftarrow g_{\psi^*}(\cdot|\hat{\mathbf{z}})$ where ψ^* pertains to the trained decoder weights and $\hat{\mathbf{z}}$ is the chosen latent space location, and $\varphi(t)$ is the probability density function of the standard normal distribution, $\mathcal{N}(0, 1)$. The expected improvement can be analytically evaluated under the GP surrogate model:

$$\text{EI}(\mathbf{z}) = \begin{cases} \underbrace{(\mu(\mathbf{z}) - f(\hat{\mathbf{y}}) - \xi)}_{(i)} \Phi(T) + \underbrace{\sigma(\mathbf{z})\varphi(T)}_{(ii)} & \text{if } \sigma(\mathbf{z}) > 0 \\ 0 & \text{if } \sigma(\mathbf{z}) = 0 \end{cases} \quad (8)$$

where,

$$T = \begin{cases} \frac{\mu(\mathbf{z}) - f(\hat{\mathbf{y}}) - \xi}{\sigma(\mathbf{z})} & \text{if } \sigma(\mathbf{z}) > 0 \\ 0 & \text{if } \sigma(\mathbf{z}) = 0. \end{cases}$$

In the above equation, $\mu(\mathbf{z})$ and $\sigma(\mathbf{z})$ are the mean and standard deviation of the surrogate GP posterior predictive at \mathbf{z} . Φ and φ are the cumulative distributive function and probability density function of the standard normal distribution, respectively.

In Eq. 8, part (i) corresponds to the exploitation term and part (ii) corresponds to the exploration term. The parameter ξ controls the amount of trade-off between exploration and exploitation (higher values ξ leads to more exploration). We set ξ to be 0.01 in all our experiments (a recommended default value). For a detailed review of the expected improvement and other popular acquisition functions we refer the reader to (Frazier, 2018; Garnett, 2023).

C OPTIMISATION AND PRACTICAL CONSIDERATIONS

To maximise the evidence lower bound, we use the Adam optimiser (Kingma & Ba, 2015), which is an adaptive learning rate method that maintains an exponentially decaying average of past gradients as well as squared gradients. The parameters that need to be optimised include the neural network weights for the encoder (ϕ) as well as decoder (ψ) and the GP kernel parameters (θ). Moreover, we separately fit the GP surrogate model for the Bayesian optimisation. In the case of mini-batch training, the optimisation steps are conducted interchangeably with natural gradient-based updates of the variational parameters.

We use PyTorch (Paszke et al., 2019) for the inference implementation which allows the computation of derivatives using automatic differentiation and we use BoTorch (Balandat et al., 2020) for Bayesian optimisation. For all experiments we set the frequency of retraining $\nu = 10$ and the stopping criterion $\eta = 0.1$. We set the number of latent dimensions to 8 for the synthetic dataset experiment, 25 for the expression reconstruction experiment, and 56 for the molecular discovery experiment.

D ABLATION STUDY

We demonstrate how our method performs with different subsets of additional auxiliary covariates. The ablations were run on the simulated data with 5000 samples and the target quantity of interest was observed for 500 samples. Fig. 6 depicts the mean target quantity of interest obtained over 100 repetitions with regenerated training data and target images.

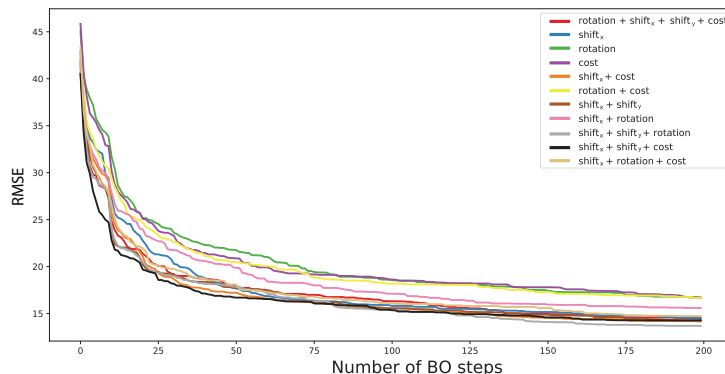


Figure 6: Results from experimenting with the choice of kernel for the synthetic dataset.

E NEURAL NETWORK ARCHITECTURES

E.1 SYNTHETIC DATASET

In the synthetic data experiment, we use the neural network architecture described in Table 1.

E.2 EXPRESSION RECONSTRUCTION

In the expression reconstruction experiment we use the Grammar VAE (Kusner et al., 2017) which is a computational model used in natural language processing and generative modelling. It combines

Table 1: Neural network architectures used in the simulated dataset.

	Hyperparameter	Value
Inference network	Dimensionality of input	52×52
	Number of convolution layers	3
	Number of filters per convolution layer	144
	Kernel size	3×3
	Stride	2
	Pooling	Max pooling
	Pooling kernel size	2×2
	Pooling stride	2
	Number of feedforward layers	2
	Width of feedforward layers	500, 50
	Dimensionality of latent space	8
	Activation function of layers	RELU
Generative network	Dimensionality of input	8
	Number of transposed convolution layers	3
	Number of filters per transposed convolution layer	256
	Kernel size	4×4
	Stride	2
	Padding	2
	Number of feedforward layers	2
	Width of feedforward layers	50, 500
Activation function of layers	RELU	

principles from VAEs and context-free grammars to learn and generate structured sequences of symbols, such as sentences, mathematical expressions, or code.

In other words, the Grammar VAE extends the VAE framework to handle structured data where the order and relationships between elements matter. Furthermore, Grammar VAE incorporates context-free grammars which define the syntax and structure of sequences. This allows the model to capture the hierarchical and compositional nature of sequences, making it well-suited for generating structured outputs. In addition to this, [Kusner et al. \(2017\)](#) proposed to represent the discrete data using a parse tree from the context-free grammar. Therefore, the model is a variational autoencoder which encodes and decodes directly to and from the generated parse trees while ensuring that the generated outputs are always valid.

In our experiments, we use a latent space dimension of 25 and make use of the neural network architecture specified in ([Kusner et al., 2017](#)).

E.3 MOLECULE OPTIMISATION

In the molecule generation experiment we use the Junction Tree VAE (JT-VAE) ([Jin et al., 2018](#)) which extends VAEs to molecular graphs by introducing a suitable encoder and decoder. The encoder learns two latent representations: one that encodes the tree structure and high-level cluster information while the other encodes fine-grained connectivity details. In particular, the model generates a molecular graph in two phases: first it generates a tree-structured scaffold over chemical sub-structures and then combines them into molecules with a graph message passing network. The molecule is encoded into two latent representations: $z = [z_{\mathcal{T}}, z_G]$ where $z_{\mathcal{T}}$ encodes the tree structure and the information of the clusters that are in the tree without fully capturing how exactly the clusters are mutually connected. The graph to capture the fine-grained connectivity is encoded by z_G .

The latent representation is then decoded back into a molecular graph in two stages. First, reproduce the junction tree using a tree decoder. Then, predict the fine-grained connectivity between the clusters in the junction tree using a graph decoder to obtain the full molecular graph. The decoder generates the molecule piece-by-piece utilising the components and how they interact instead of assembling the molecule atom-by-atom and/or through chemically invalid intermediaries.

The graph encoder is a graph message passing network (graph neural networks), the tree encoder is a tree message passing network (related to RNNs and tree-LSTM), the junction tree is reconstructed

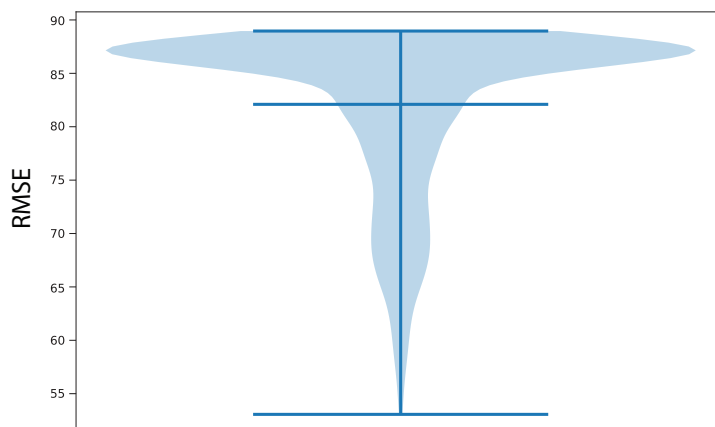
918 using a structured tree decoder, and the fine-grained cluster details are obtained using a graph decoder.
919 Furthermore, the latent space dimension is 56 (tree and graph representations are 28 dimensions
920 each).

921 The key benefit is the incremental expansion of the molecule while maintaining chemical validity at
922 every step. Furthermore, each molecule is built from sub-graphs chosen out of a vocabulary of valid
923 components. In this work, we use the same neural network architecture specification as in (Jin et al.,
924 2018). Our proposed model is agnostic to the choice of the underlying neural network architecture.
925

926 F SUPPLEMENTARY IMAGES



930
931
932
933
934
935
936
937
938
939
940
941
942
943
944
945
946
947
948 Figure 7: A random sample of digits (from the the synthetic dataset) that have been rotated and
949 shifted along the x and y axis.



951
952
953
954
955
956
957
958
959
960
961
962
963
964
965
966
967 Figure 8: Violin plot visualising the distribution of the quantity of interest in an instance of the
968 synthetic dataset.

969
970
971

972
 973
 974
 975
 976
 977
 978
 979
 980
 981
 982
 983
 984
 985
 986
 987
 988
 989
 990
 991
 992
 993
 994
 995
 996
 997
 998
 999
 1000
 1001
 1002
 1003
 1004
 1005
 1006
 1007
 1008
 1009
 1010
 1011
 1012
 1013
 1014
 1015
 1016
 1017
 1018
 1019
 1020
 1021
 1022
 1023
 1024
 1025

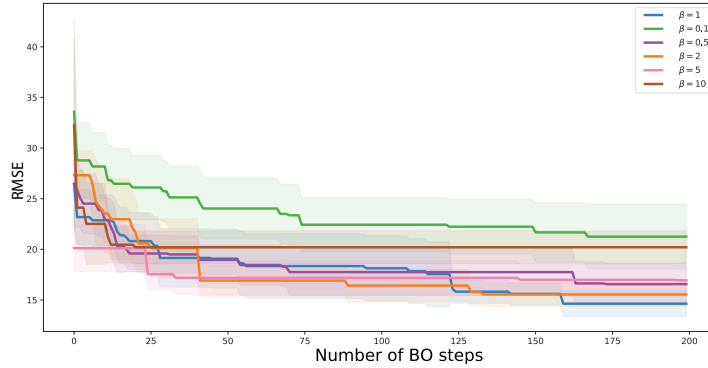


Figure 9: A demonstration of the effect of β (as in β -VAE (Higgins et al., 2017)) on the model performance in the synthetic dataset.

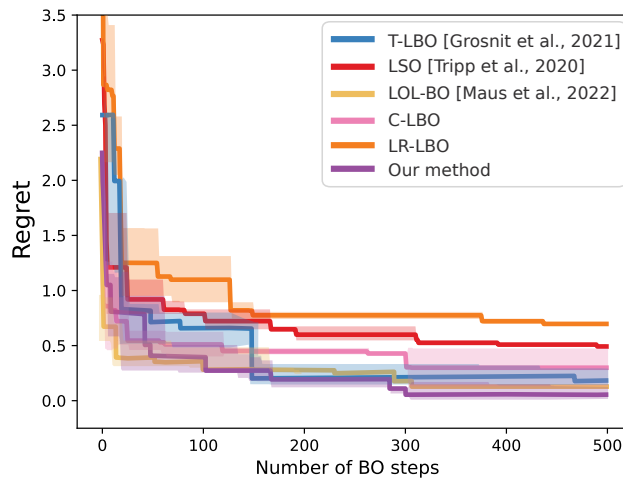


Figure 10: Results from the expression reconstruction experiment. The mean regret achieved by our method compared to competing methods over 5 repetitions is visualised together with the 95% confidence interval (shaded region). **Lower values are better.**

1026
1027
1028
1029
1030
1031
1032
1033
1034
1035
1036
1037
1038
1039
1040
1041
1042
1043
1044
1045
1046
1047
1048
1049
1050
1051
1052
1053
1054
1055
1056
1057
1058
1059
1060
1061
1062
1063
1064
1065
1066
1067
1068
1069
1070
1071
1072
1073
1074
1075
1076
1077
1078
1079

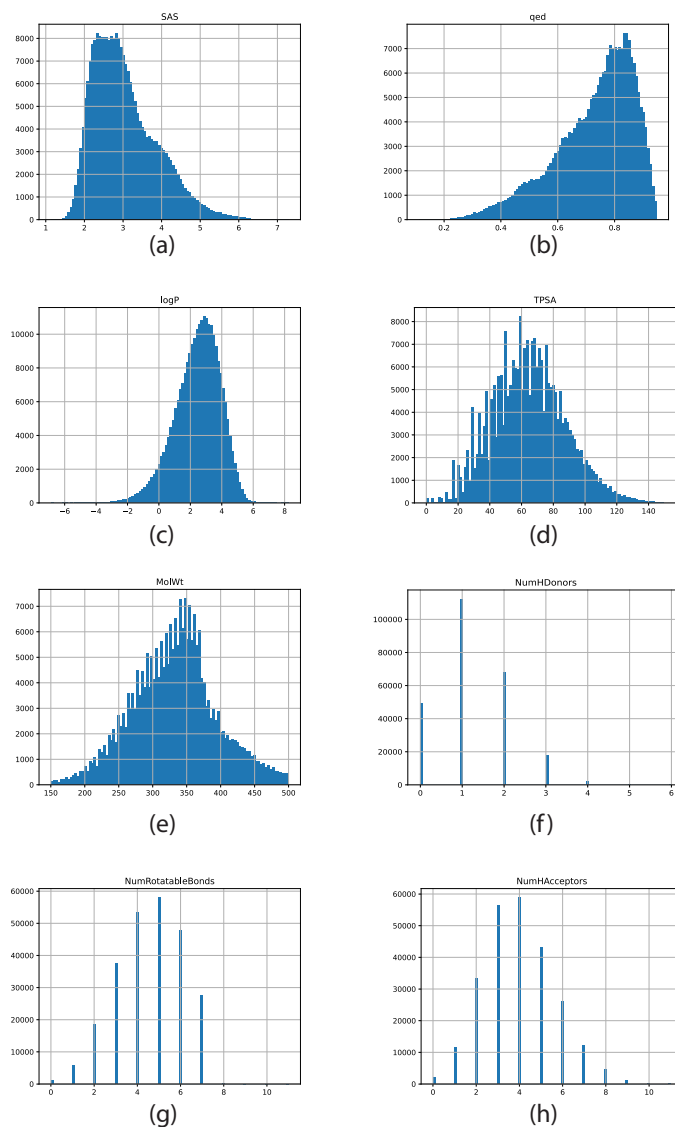


Figure 11: Histograms visualising the distribution of the properties in the ZINC-250K dataset.

1080
 1081
 1082
 1083
 1084
 1085
 1086
 1087
 1088
 1089
 1090
 1091
 1092
 1093
 1094
 1095
 1096
 1097
 1098
 1099
 1100
 1101
 1102
 1103
 1104
 1105
 1106
 1107
 1108
 1109
 1110
 1111
 1112
 1113
 1114
 1115
 1116
 1117
 1118
 1119
 1120
 1121
 1122
 1123
 1124
 1125
 1126
 1127
 1128
 1129
 1130
 1131
 1132
 1133

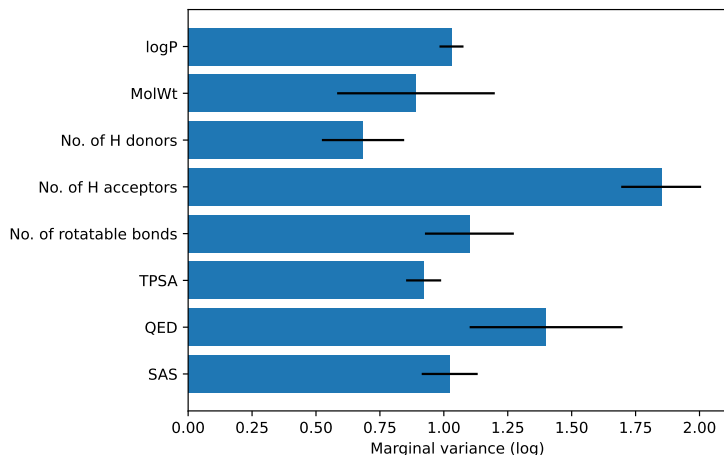


Figure 12: *Marginal variance of the additive components in the molecule discovery experiment.* We visualise the mean and standard deviation of the marginal variance for each of the kernel components across the 56 latent dimensions. This pertains to an additive kernel over all the covariates.

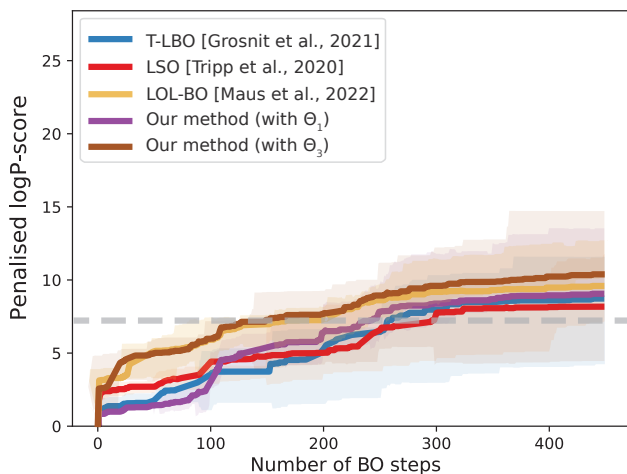


Figure 13: *Results from the molecule optimisation experiment with the penalised logP observed for only 0.1% of the data.* The mean penalised logP score over 10 repetitions is visualised together with the 95% confidence interval (shaded region). The grey line pertains to the highest penalised logP score in the training set. Θ_1 pertains to an additive kernel over all 7 covariates and the partially observed target quantity, and Θ_3 pertains to an additive kernel over only the 5 additional properties that were calculated with RDKit (and does not include the partially observed target quantity). The overall performance of all the methods decrease because the Bayesian optimisation has fewer number of points to fit the surrogate model with. However, it is interesting to note that our method with an additive kernel that does not include the quantity of interest performs the best (by a small margin). The other approaches make use of the quantity of interest (penalised logP) while fitting the model. We believe that this demonstrates that our model (with Θ_3) is able to learn meaningful latent representations without making use of the partially observed target quantity of interest. **Higher values are better.**

1134
1135
1136
1137
1138
1139
1140
1141
1142
1143
1144
1145
1146
1147
1148
1149
1150
1151
1152
1153
1154
1155
1156
1157
1158
1159
1160
1161
1162
1163
1164
1165
1166
1167
1168
1169
1170
1171
1172
1173
1174
1175
1176
1177
1178
1179
1180
1181
1182
1183
1184
1185
1186
1187

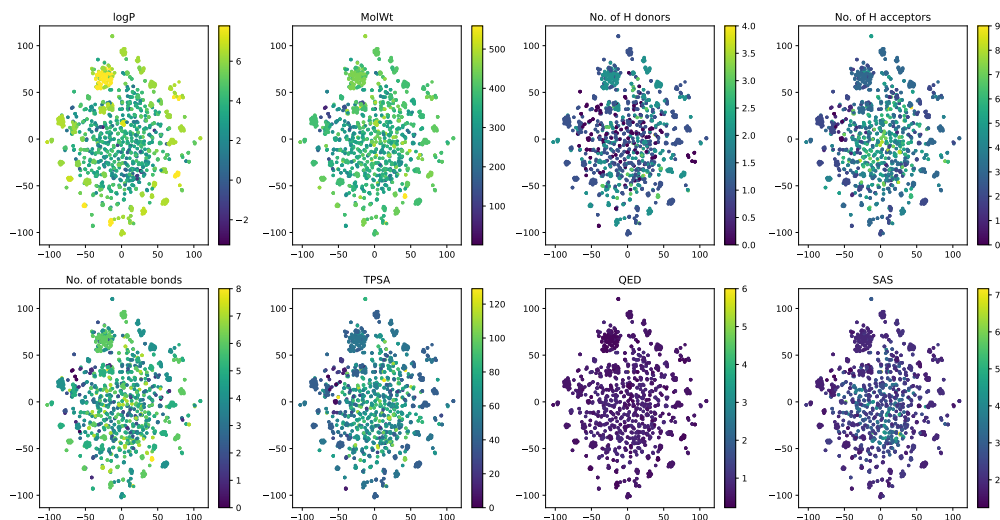


Figure 14: *Visualisation of the latent space in the molecule discovery experiment.* We performed a projection of the latent space from 56 dimensions down to two dimensions using t-SNE and using the validation dataset for convenience. The latent embedding is coloured by the respective molecular properties. The proposed model learns a latent embedding that changes smoothly with respect to the target quantity as well as with respect to the additional covariates (noting again that the visualisation corresponds to a 2-D t-SNE embedding).

G SUPPLEMENTARY TABLES

Table 2: Average run time / wall clock time. In the synthetic dataset experiment 200 BO steps are performed and in the molecule discovery experiment 450 BO steps are performed.

Method	Experiment	Configuration	GPU type	CPU type	Runtime (avg.)
Our method	Synthetic data (5000 obs.)	Kernel Θ_1	AMD MI250x	AMD EPYC "Trento"	152 mins
		Kernel Θ_2	AMD MI250x	AMD EPYC "Trento"	140 mins
		Kernel Θ_3	AMD MI250x	AMD EPYC "Trento"	163 mins
	Expression reconstruction	-	Nvidia Tesla V100	Intel Xeon Gold 6134	1064 mins
		Kernel Θ_1	Nvidia Tesla V100	Intel Xeon Gold 6134	1682 mins
		Kernel Θ_2	Nvidia Tesla V100	Intel Xeon Gold 6134	1641 mins
Molecular discovery	-	Nvidia Tesla V100	Intel Xeon Gold 6134	1668 mins	
	Kernel Θ_1	-	AMD MI250x	AMD EPYC "Trento"	102 mins
	Kernel Θ_2	-	Nvidia Tesla V100	Intel Xeon Gold 6134	723 mins
LSO (Tripp et al., 2020)	Synthetic data (5000 obs.)	-	AMD MI250x	AMD EPYC "Trento"	102 mins
	Expression reconstruction	-	Nvidia Tesla V100	Intel Xeon Gold 6134	723 mins
	Molecular discovery	-	Nvidia Tesla V100	Intel Xeon Gold 6134	1038 mins
T-LBO (Grosnit et al., 2021)	Expression reconstruction	-	Nvidia Tesla V100	Intel Xeon Gold 6134	918 mins
	Molecular discovery	-	Nvidia Tesla V100	Intel Xeon Gold 6134	1582 mins
LOL-BO (Maus et al., 2022)	Expression reconstruction	-	Nvidia Tesla V100	Intel Xeon Gold 6134	802 mins
	Molecular discovery	-	Nvidia Tesla V100	Intel Xeon Gold 6134	845 mins

H LIMITATIONS

While our method proposes a novel approach to performing high-dimensional Bayesian optimisation efficiently, it shares several of the limitations of standard VAEs. For example:

- It can be challenging to model complex (or multi-modal) data.
- The performance is dependent on the expressiveness of the chosen neural network architecture for the encoder and decoder.
- The latent space is assumed to follow a Gaussian distribution which may not hold true for all datasets.
- Sensitivity to the hyperparameter values such as dimensionality of the latent space, weight of the KL divergence (β), minibatch size, etc.

Furthermore, in GP prior VAEs, the choice of the auxiliary covariates used for the GP prior needs to be done empirically. Despite these limitations, GP prior VAEs have been successful in various applications and have contributed to advances in generative modelling and unsupervised representation learning.

I BROADER IMPACTS

Generative machine learning models have gained significant attention in recent times. In this work, we make use of the variational autoencoder which has been primarily used for representation learning, imputation, and data generation tasks. However, VAEs (and deep generative models in general) present several societal implications that extend beyond the scope of academia and research. Furthermore, they present ethical considerations due to their potential malicious applications including contributing to misinformation and possible privacy concerns. Robust frameworks as well as guidelines need to be established to address these concerns and to ensure the responsible deployment of generative machine learning technologies. It is essential to navigate the ethical concerns and to ensure the responsible use of deep generative models for the betterment of society.

REFERENCES

Maximilian Balandat, Brian Karrer, Daniel R. Jiang, Samuel Daulton, Benjamin Letham, Andrew Gordon Wilson, and Eytan Bakshy. BoTorch: A Framework for Efficient Monte-Carlo Bayesian Optimization. In *Advances in Neural Information Processing Systems 33*, 2020. URL <http://arxiv.org/abs/1910.06403>.

- 1242 Peter I Frazier. Bayesian optimization. In *Recent advances in optimization and modeling of*
1243 *contemporary problems*, pp. 255–278. Informa, 2018.
- 1244 Roman Garnett. *Bayesian optimization*. Cambridge University Press, 2023.
- 1246 Antoine Grosnit, Rasul Tutunov, Alexandre Max Maraval, Ryan-Rhys Griffiths, Alexander I Cowen-
1247 Rivers, Lin Yang, Lin Zhu, Wenlong Lyu, Zhitang Chen, Jun Wang, et al. High-dimensional
1248 bayesian optimisation with variational autoencoders and deep metric learning. *arXiv preprint*
1249 *arXiv:2106.03609*, 2021.
- 1250 James Hensman, Nicolo Fusi, and Neil D Lawrence. Gaussian processes for big data. In *Proceedings*
1251 *of the 29th Conference on Uncertainty and Artificial Intelligence*, 2013.
- 1253 Wengong Jin, Regina Barzilay, and Tommi Jaakkola. Junction tree variational autoencoder for
1254 molecular graph generation. In *International Conference on Machine Learning*, pp. 2323–2332.
1255 PMLR, 2018.
- 1256 Diederik P. Kingma and Jimmy Ba. Adam: A method for stochastic optimization. In *3rd International*
1257 *Conference on Learning Representations, ICLR*, 2015.
- 1259 Diederik P. Kingma and Max Welling. Auto-encoding variational bayes. In *2nd International*
1260 *Conference on Learning Representations, ICLR*, 2014.
- 1261 Matt J Kusner, Brooks Paige, and José Miguel Hernández-Lobato. Grammar variational autoencoder.
1262 In *International Conference on Machine Learning*, pp. 1945–1954. PMLR, 2017.
- 1264 Natalie Maus, Haydn T Jones, Juston S Moore, Matt J Kusner, John Bradshaw, and Jacob R Gardner.
1265 Local latent space bayesian optimization over structured inputs. *Advances in Neural Information*
1266 *Processing Systems*, 2022.
- 1267 Adam Paszke, Sam Gross, Francisco Massa, Adam Lerer, James Bradbury, Gregory Chanan, Trevor
1268 Killeen, Zeming Lin, Natalia Gimelshein, Luca Antiga, et al. PyTorch: An imperative style,
1269 high-performance deep learning library. In *Advances in Neural Information Processing Systems*,
1270 *NeurIPS*, 2019.
- 1271 Siddharth Ramchandran, Gleb Tikhonov, Kalle Kujanpää, Miika Koskinen, and Harri Lähdesmäki.
1272 Longitudinal variational autoencoder. In *International Conference on Artificial Intelligence and*
1273 *Statistics*, pp. 3898–3906. PMLR, 2021.
- 1275 Siddharth Ramchandran, Gleb Tikhonov, Otto Lönnroth, Pekka Tiikkainen, and Harri Lähdesmäki.
1276 Learning conditional variational autoencoders with missing covariates. *Pattern Recognition*, 147:
1277 110113, 2024.
- 1278 Michalis Titsias. Variational learning of inducing variables in sparse gaussian processes. In *Artificial*
1279 *Intelligence and statistics*, pp. 567–574. PMLR, 2009.
- 1281 Austin Tripp, Erik Daxberger, and José Miguel Hernández-Lobato. Sample-efficient optimization in
1282 the latent space of deep generative models via weighted retraining. *Advances in Neural Information*
1283 *Processing Systems*, 33:11259–11272, 2020.
- 1284
1285
1286
1287
1288
1289
1290
1291
1292
1293
1294
1295